Mirrors and M1 Unit

The first primary mirror blank has been delivered to REOSC and the pads for the axial supports have been glued on the back. The manufacturing of other blanks by Schott proceeds as planned. Two parallel contracts were issued for the design of the mirror cell. The Preliminary Design Review will take place at the beginning of next year.

M2 Unit

The call for tenders has been issued and the tenders are expected in mid-December. The requirements include a fast guiding mode (field stabilization) and a chopping mode for frequencies up to 5 Hz and amplitude of up to 1 arcminute.

Coating Plant

The technical specifications and statement of work for the Call for Tenders have been completed. The specifications are based on a sputtering process. The start of the contract is expected to be May 1994.

Washing Unit and Cleanroom

The specifications and statement of work for the call for tenders is being prepared. The contract for the washing unit will include the pilot washing unit (for the 3.6-metre mirrors) for La Silla. Cleanroom specifications have been prepared. The cleanroom will comprise both the coating and washing unit for the 8-m mirrors.

Cassegrain and Nasmyth Adapters

The conceptual design has been completed and the call for tenders will be sent out early in 1994 after analysis of the results of a preliminary enquiry. A call for tenders is running for the procurement of CCD cameras for autoguiding and wavefront sensing applications.

Coudé Station

The concept is based on a large turntable on which all the coudé station equipment is fixed. It is used to compensate the field rotation for coudé instruments and to position the collimating units to be used for the different types of beam combinations. The contract for the construction of turntables has been issued.

Adaptive Optics

An optimization study has permitted the finalization of the essential parameters necessary for the establishment of specifications.

Handling Aspects

A new concept for the M1 handling tool has been developed. The principle is a hydraulic whiffle tree. The geometry is identical to that of the REOSC tool. The M1 handling tool will include the lifting system and will form a self-standing unit in the Mirror Maintenance Building.

VLTI System Level

A number of studies at system level are currently being carried out or have been completed. These studies are important for assessing the overall performance of the VLTI as well as for the specification of VLTI subsystems, such as the delay lines. Studies include:

- Control model of delay line/fringe sensor
- Structural deformation of unit telescopes under wind loads
- Study of acoustic noise inside UT enclosures
- Study of thermal environment in VLTI facilities
- Measurements of ground transfer functions on Paranal

Auxiliary Telescopes

Calls for tenders for the design, manufacture, test in Europe, transport to and erection in Chile of three auxiliary telescopes and equipment for 11 stations were sent to industry in July 1993.

Beam Combiner System

An in-house design study of the beam combiner is nearing completion. The main objective of the study is a conceptual design which allows the assessment of the interface to the civil engineering infrastructure and understanding of the tradeoffs between various concepts for the homothetic mapping.

Instrumentation

The VLT Medium Resolution Spectrometer/Imager (ISAAC) reached the Final Design Review (FDR). The CONICA (High Resolution Near Infrared Camera) and FORS (Focal Reducer Spectrograph) are approaching the FDR stage. The UV-Visual Echelle Spectrograph (UVES) completed the Preliminary Design Review in October. The Multi-Fiber Area Spectrograph (FUEGOS) is being studied by a consortium composed of the Observatoire de Meudon, the Observatoire de Genève, the Observatoire de Toulouse and the Osservatorio di Bologna. The Phase A study ended in October and is being reviewed by ESO technical staff. The Mid-Infrared Image Spectrometer is being studied by the Service d'Astrophysique CEA/DAPNIA and is making progress in Phase A.

First Light from the NTT Interferometer

T.R. BEDDING, O. VON DER LÜHE and A.A. ZIJLSTRA, ESO
A. ECKART and L.E. TACCONI-GARMAN, MPE Garching, Germany

It is not obvious that placing a mask over a telescope and blocking most of the light will improve its imaging performance. Yet several groups have done just this in an effort to overcome the limits of atmospheric seeing and achieve the best angular resolution from large telescopes such as the 4.2-m WHT, the 3.9-m AAT, the Hale 5-m and the Mayall 4-m at Kitt Peak. Aperture masking has mainly been used for bright sources having reasonably simple structure. Fortunately, there are some very interesting objects that satisfy these criteria: cool giant stars, whose large angular diameters (up to ~0.05″) make them ideal targets for big telescopes. Aperture masking has so far allowed detection of convective hot spots on the red supergiant α Ori and asymmetries in the atmosphere of Mira (e.g., Wilson et al. 1992; Haniff et al. 1992).

This article describes aperture-masking observations of cool giants with the 3.5-m NTT in the near infrared (1.5 μm). We chose the infrared because, although the angular resolution is somewhat poorer than at visible wavelengths, the stars are much brighter and the atmospheric seeing is more favourable.

Before describing our observations, we give a brief introduction to the techniques involved.

Optical/IR Interferometry

To produce images that have high angular resolution one must overcome the seeing. This means compensating for perturbations in the wavefront of the light that result from its passage through the atmosphere. These perturbations arise because the refractive index of the atmosphere is continually fluctuating, primarily due to turbulent mixing of regions of air with differing temperatures. The incoming wavefront can be thought of as being made up of a large number of patches, each having a diameter of r_0, where the wavefront is approximately flat across each patch. The quantity r_0 determines the seeing: at a wavelength λ, the seeing disk has a FWHM of about $1.2\,\lambda/r_0$ (e.g., r_0 = 15 cm at 550 nm for 1″ seeing).

Adaptive optics seeks to compensate for wavefront perturbations in real time using a small deformable mirror. Provided the mirror has enough actuators (one for every r_0-sized patch on the pupil), it is possible to place most of the light in a diffraction-limited core. Of course, one also requires sufficient photons per r_0-patch to measure the wavefront and calculate the correction.[1]

It is possible to achieve high angular resolution passively (i.e. without adaptive optics), provided one has a fast detector. This involves recording the distorted image in a succession of short exposures, each of which "freezes" the seeing, and processing them off-line. This is the basis of speckle interferometry. Each short-exposure image contains high-resolution information which can be extracted via a Fourier transform and calibrated using similar observations of a nearby unresolved star.

Aperture masking is identical to speckle interferometry, except that one places a mask over the telescope pupil. The mask may consist of a small number of holes arranged in a non-redundant pattern (i.e., so that all baseline vectors are distinct). Alternatively, it may be partially redundant, such as an annulus or a slit. The pros and cons of aperture masking have been discussed elsewhere (Haniff & Buscher 1992; Buscher & Haniff 1993; Haniff 1993) and here we simply try to summarize the main arguments.

[1] *Adaptive* optics is not the same as *active* optics. The latter involves adjusting the primary mirror to correct for telescope flexure, etc., and the corrections are necessarily made on a much slower timescale. This type of correction produces excellent long-exposure images, but cannot be used for real-time seeing compensation.

Why Use an Aperture Mask?

Each r_0-sized patch on the pupil has an unknown phase error, corresponding to the unknown thickness of atmosphere above it. Each *pair* of patches forms an interferometer that measures a particular spatial frequency on the sky. With an un-masked pupil there are many different pairs measuring a given spatial frequency. Each one contributes a different phase error, so that many fringe patterns with the same spatial frequency are superimposed on the detector with different position offsets. The resultant fringe power will be the sum of these randomly-phased contributions. The problem is that the wavefront errors are different in every short-exposure image, so the final fringe power, being the sum of a random walk, will also fluctuate. This introduces so-called atmospheric noise in the power spectrum. A non-redundant aperture mask, in which no baseline is sampled more than once, eliminates atmospheric noise. This is particularly important in the infrared, where the large numbers of photons mean that atmospheric noise usually dominates over photon noise.

Another advantage of non-redundant aperture masking is that it improves the accuracy with which one can correct for variations in atmospheric seeing, something which is often the limiting factor in high-resolution imaging. This is because a pupil composed of subapertures each having size $\lesssim r_0$ is quite insensitive to changes in the actual value r_0. Of course, a mask also reduces the light level and restricts observations to bright objects. But for those objects, there is an additional advantage if the light being discarded does not carry useful information. This last point becomes clear if one imagines observing an object which is only barely resolved by the full telescope aperture. In this case, the "useful" light comes from the outer parts of the pupil and the remainder only serves to add noise to the signal we are interested in. By using a mask, one can effectively increase the resolving power of the telescope by giving more emphasis to high spatial frequencies.

A big drawback of using a non-redundant mask with a small number of holes is the poor coverage of spatial frequencies. A good compromise in the photon-rich infrared regime is an annular mask. This has full spatial frequency coverage while being minimally redundant: roughly speaking, each baseline is measured twice. Furthermore, a thin annulus largely retains the other advantages mentioned above, namely accurate calibration and enhanced resolution. However, an annular mask is not a good choice in the visible regime, where photon noise generally dominates over atmospheric noise. Here, Buscher & Haniff (1993) advocate the use of a long slit.

Figure 1: *To change between masks, the NTT was tilted to 15° from the horizontal and the mirror cover (grey) was partially closed. Here, Oskar von der Lühe (left) and Tim Bedding (right) stand on the telescope structure and show off the 7-hole mask. The black circle behind their heads is the annular mask attached to the M3 baffle. Andreas Eckart is standing at floor level.*

We do not wish to give the impression that masking a telescope is always the best strategy. In some situations, however, there are powerful arguments for doing so and these issues are discussed more fully in the references. To summarize, an aperture mask with non-redundant holes provides more accurately calibrated measurements at the full diffraction limit, but at the expense of lower sensitivity and poorer spatial-frequency coverage. As noted above, an annular mask should be a good compromise in the infrared, but this method has so far only been tested on binary stars (Haniff et al. 1989).

Masking the NTT

Our observations were made on the NTT in August 1993, using the SHARP infrared camera (Eckart et al. 1991). In order to sample the images fully at the diffraction limit at the J band, it was necessary to magnify the image scale. We did this by placing a focal expander just in front of the dewar window. This device, which we named COSHARP, consisted of a pair of lenses mounted in an aluminium tube. COSHARP performed perfectly and we wish the same success to its more expensive space-based cousin.

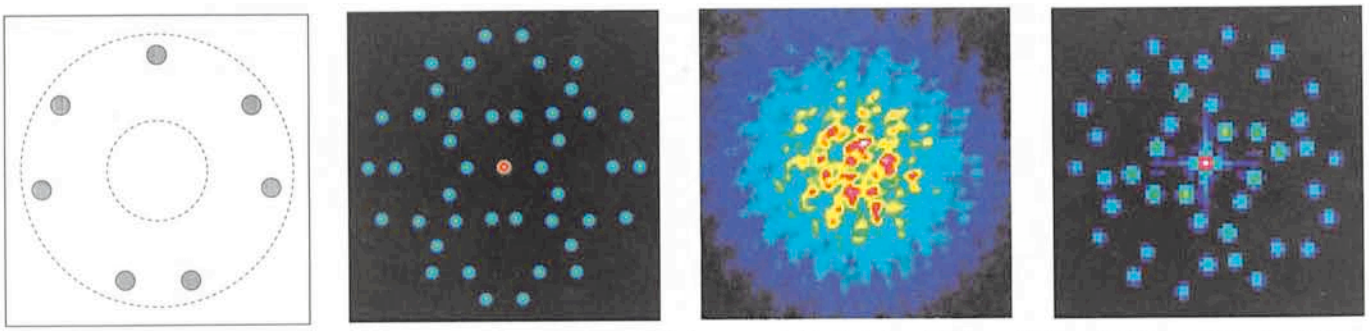

Figure 2: *(a) The 7-hole non-redundant mask, with the pupil of the NTT shown as dashed circles. (b) Theoretical spatial-frequency coverage. The central red dot is the origin and the other points (in symmetrical pairs) show the 21 different baselines.*
(c) Typical 0.1-s exposure of a bright star. The envelope corresponds to the airy disk of a single hole and fringes from the interferometric array are clearly visible. The image is 2.9″ across.
(d) The average power spectrum of 200 interferograms like the one in (c). Since the telescope has an alt-azimuth mount, the orientation of the pattern varies with the rotation angle of the mask with respect to the sky.

We observed several red giants and Mira variables using both an annular mask and a 7-hole non-redundant mask. Placing a full-sized mask over the primary mirror of a large telescope is rather difficult, especially if you want to change between different masks during the night. The solution adopted by most observers is to place the mask inside the instrument at an image of the telescope pupil. Re-imaging the pupil to a diameter of ~20 mm with a lens allows one to use a correspondingly smaller mask, which is very convenient but requires extra optics to be inserted in the system. With SHARP on the NTT, this was not practicable.

The NTT is a compact alt-azimuth telescope in a small enclosure, making it quite easy to access the telescope structure. This allowed us to place the masks on the baffle in front of Mirror 3, at which point the converging f/11 beam has a diameter of 45 cm. The masks were made from 5 mm thick black PVC and, by bolting a mounting ring to the M3 baffle, we were able to attach and remove them very easily. To reach the M3 baffle, we drove the telescope to its lowest elevation (15°), partly closed the primary mirror cover and climbed onto the telescope structure. The whole process of changing the mask took two people about 5 minutes (see Figure 1).

The mirror cover of the NTT opens like a pair of sliding doors, which makes it useful as a secure handhold. We note in passing that this mirror cover can easily be used to create a *slit* mask, simply by opening the cover to the desired width. As mentioned above, a slit mask can be used for interferometry at visible wavelengths.

The design of the 7-hole mask is shown in Figure 2(a). When projected on the entrance pupil of the NTT, the holes have a diameter of 25 cm and lie on a circle of diameter 3.05 m. We did not use the full diameter of the pupil (3.5 m) in order to avoid vignetting that would arise from the mask not being exactly at the pupil plane. Figure 2(b) shows the two-dimensional spatial frequency coverage. The arrangement of the holes is based on a design by Cornwell (1988), except that we moved the lower pair of holes closer together to make the radially-averaged coverage of spatial frequencies more uniform. Figures 2(c) and (d) show data from a bright star. The signal in the power spectrum is attenuated relative to the theoretical pattern (2b), mainly due to seeing decorrelation during each 0.1-s exposure. This exposure time, which was set by the detector system, is a little long and we plan to install a fast shutter for future observations.

The annular mask (Figure 3) has an effective outer diameter of 3.3 m and a width of 20 cm. The transfer function (Figure 3b) gives strong emphasis to high spatial frequencies. In the mid-frequency range the transfer function is a factor of ~7 below that of the unmasked telescope. However, in the presence of seeing, the signal from the unmasked telescope is strongly attenuated, while that from the annular mask (Figure 3d) is less severely affected.

Results and Future Prospects

Despite poor weather, we obtained good observations of several southern red giants and Miras that we would expect to have large angular diameters.

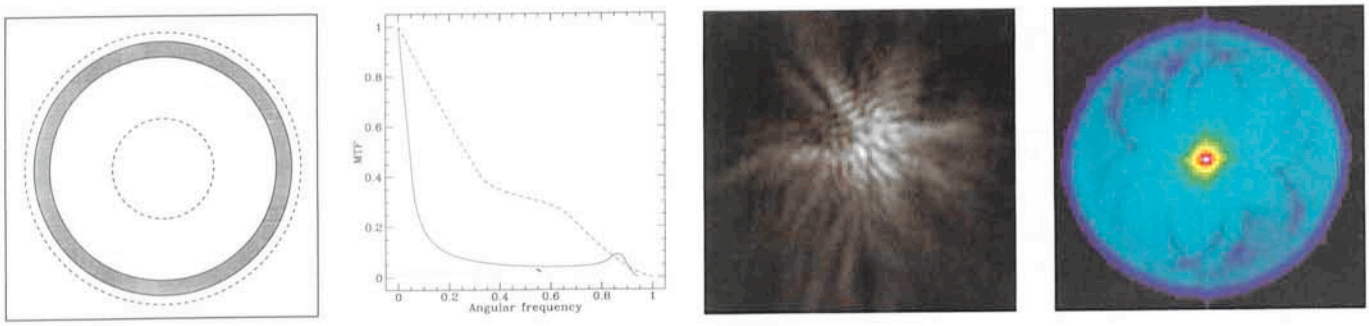

Figure 3: *(a) The annular mask, with the pupil of the NTT shown as dashed circles.*
(b) Radial cuts through the NTT modulation transfer function in the absence of seeing effects. The solid curve is for the annular mask and the dashed curve is without a mask (but including the telescope's central obstruction). An angular frequency of 1 corresponds to the diffraction limit of the full 3.5-m aperture.
(c) Typical 0.1-s exposure of a bright star, showing many small speckles. The image is 2.9″ across.
(d) The average power spectrum of 500 interferograms like the one in (c). The origin of the spatial frequency domain is at the centre, where the signal is strongest. The arc-like features are due to the telescope spiders and also to a deposit on M3 courtesy of the bird life on La Silla.

Preliminary analysis of the data indicates that these stars are resolved and that they probably rival Betelgeuse and Mira in angular size. If this turns out to be the case, we will be able to look for evidence of asymmetries and surface features on these stars.

The number of stars that can be resolved by 4-m-class telescopes is small, but the results so far have proved very interesting. The new generation of 8–10-m telescopes will give a big improvement in angular resolution, and masking observations similar to those we have described should allow detailed study of stars with large angular diameters. At the moment, however, there are always practical difficulties with aperture masking. We therefore hope that future instruments will be designed to contain a reimaged pupil at which masks can be easily inserted.

We thank Reiner Hofmann for making COSHARP, Gerardo Ihle and the staff in the La Silla workshop for making the masks, and telescope operator Francisco Labraña for excellent support during the observations.

References

Buscher, D.F., & Haniff, C.A., 1993, *J. Opt. Soc. Am. A.* **10**, 1882.

Cornwell, T.J., 1988, *IEEE Trans. Antennas and Propagation* **36**, 1165.

Eckart, A., Hofmann, R., Duhoux, P., Genzel, R., & Drapatz, S., 1991, *The Messenger* **65**, 1.

Haniff, C.A., & Buscher, D.F., 1992, *J. Opt. Soc. Am. A.* **9**, 203.

Haniff, C.A., Buscher, D.F., Christou, J.C., & Ridgway, S.T., 1989, *MNRAS* **241**, 51P.

Haniff, C.A., Ghez, A.M., Gorham, P.W., Kulkarni, S.R., Matthews, K., & Neugebauer, G., 1992, *AJ* **103**, 1662.

Haniff, C.A., 1993, Speckle v non-redundant masking. In: Robertson, J.G., & Tango, W.J. (eds.), *Proc. IAU Symp. 158, Very High Angular Resolution Imaging*, Sydney, Australia, January 1993, in press.

Wilson, R.W., Baldwin, J.E., Buscher, D.F., & Warner, P.J., 1992, *MNRAS* **257**, 369.

Optical Gyro Encoder Tested on the NTT

H. DAHLMANN, B. HUBER, W. SCHRÖDER, L. SCHÜSSELE, H. ZECH, Fachhochschule Offenburg and Steinbeis Transfer Zentrum Physikalische Sensorik, Offenburg, Germany

M. RAVENSBERGEN, European Southern Observatory

The prototype of the optical gyro encoder (see [1] and [2]) has been successfully tested on the NTT telescope in the period of 5 to 10 September 1993. Day time tests until 20 September proved the repeatability of the measurements. The tests confirmed the specifications of the encoder and qualified this type of angular encoder for the use in an optical telescope.

The optical gyro encoder (OGE) consists of two gyros:

1. A ring laser gyro. This gyro consists of a triangular or square light path with mirrors in the corners. Laser light from an ionizing laser source (e.g. HeNe) is emitted in the 2 directions of the light path and the resulting interference pattern is measured.
   The light path is made in a glass block with a thermal expansion coefficient of zero. It has therefore a very stable scale factor but the resolution is not sufficient.
2. A fiber optic gyro. This gyro consists of a polarization maintaining fiber, which is wound on a coil. A light source emits light in the two directions of the coil, and the interference pattern is measured. Compared with a ring laser gyro with the same enclosed area for the light path, the sensitivity multiplies with the number of turns. This results in an excellent resolution and low noise. On the other hand, the scale factor is not sufficient because of imperfections in the optical elements and thermal effects.

In principle, the OGE integrates the signal of the ring laser gyro and compensates it for misalignments and earth rotation in order to get the angles in telescope coordinates. The ring laser gyro data are also used to stabilize the fiber optic gyro. The data collection was however done for the two gyros individually and the data were evaluated off-line in order to find the best integration time constant.

The OGE data were transformed into altitude/azimuth coordinates according to its system equations and calibration data. This was compared with the readings of the altitude and azimuth encoders of the NTT.

The OGE was first mounted on the

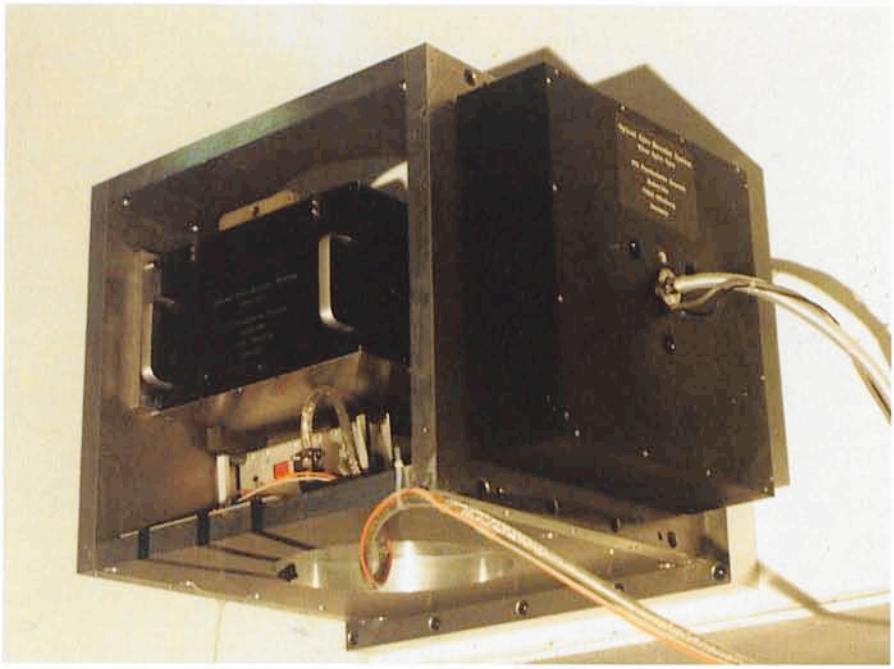

The optical gyro encoder mounted on the NTT centre piece (altitude axis). The ring laser with its front-end electronics is mounted in the box, while the fiber gyro is mounted on the right-hand plate. Dimensions of the mounting box are about 45 × 45 × 45 cm. The axis of the optical gyro encoder is from left to right on this picture.